CATÓLICA
ESCOLA SUPERIOR DE BIOTECNOLOGIA
PORTO

3D BIOPRINTING USING TISSUE-DERIVED BIOINKS

by

Camila Vilar Baptista

November 2025

CATÓLICA
ESCOLA SUPERIOR DE BIOTECNOLOGIA
PORTO

3D BIOPRINTING USING TISSUE-DERIVED BIOINKS

Thesis presented to Escola Superior de Biotecnologia of the Universidade Católica Portuguesa to fulfil the requirements of Master of Science degree in Biomedical Engineering

by

Camila Vilar Baptista

Supervisor: Doctor Estelle Palierse

Tutor: Doctor Viviana Ribeiro

November 2025

Resumo

A bioimpressão 3D permite a criação detalhada de estruturas semelhantes a tecidos utilizando biotintas feitas de biomateriais e células. A matriz extracelular descelularizada (dECM), extraída de tecidos naturais, fornece bioatividade que ajuda as células a sobreviver e a responder especificamente ao tecido.

Nesta tese, descelularizámos pele de porco para criar um hidrogel a uma concentração de 2.5 $mg.ml^{-1}$. Testámos o hidrogel como uma potencial biotinta para bioimpressão baseada em extrusão. Para verificar se o processo de descelularização foi bem-sucedido, realizámos ensaios bioquímicos. Esses testes mostraram que os principais componentes da matriz extracelular (ECM) foram preservados em sua maioria.

O hidrogel apresentou comportamento de diluição por cisalhamento e gelificação adequados para impressão. No entanto, a sua integridade estrutural limitou-se a duas camadas, o que indicou uma fraca estabilidade mecânica. Os fibroblastos L929 permaneceram vivos e mostraram propagação contínua às 24 horas e 72 horas.

Estes resultados destacam o potencial das biotinas dECM suínas e enfatizam a necessidade de estratégias, tais como reticulação biocompatível, para melhorar o suporte mecânico a longo prazo.

Palavras-Chave: hidrogéis derivados da pele de porco, descelularização, matriz extracelular, bioimpressão baseada em extrusão, engenharia de tecidos.

Abstract

3D bioprinting allows for the detailed creation of tissue-like structures using bioinks made from biomaterials and cells. Decellularized extracellular matrix (dECM), extracted from natural tissues, provides bioactivity that helps cells survive and respond specifically to the tissue.

In this thesis, we decellularized pig skin to create a hydrogel at a concentration of 2.5 $mg.ml^{-1}$. We tested it as a potential bioink for extrusion-based bioprinting. To check if the decellularization process was successful, we conducted biochemical assays. These tests showed that the key components of the extracellular matrix (ECM) were mostly preserved.

The hydrogel showed shear-thinning behavior and gelation suitable for printing. However, its structural integrity was limited to two layers, which indicated weak mechanical stability. L929 fibroblasts remained alive and showed continued spreading at 24 hours and 72 hours.

These results highlight the potential of porcine dECM bioinks and emphasize the need for strategies, such as biocompatible crosslinking, to enhance long-term mechanical support.

Key-words: porcine skin-derived hydrogels, decellularization, extracellular matrix, extrusion-based bioprinting, tissue engineering.

Acknowledgements

This thesis work was achieved thanks to the support of various people whom I would like to acknowledge gratefully.

First and foremost, I am deeply grateful to my supervisor, Estelle Palierse, for your steady support, thoughtful guidance, and constant willingness to help whenever needed. I couldn't have asked for a better supervisor to be on this journey with.

To Professor Cecilia Persson, I would like to thank you for giving me the opportunity to work in her group, the BioMaterial Systems Group.

To all the BMS and EMBLA members, thank you all for the help and company during the last couple of months.

Special thanks to the Erasmus+ programme and the funding grant that made this international research experience possible. I would also like to thank my co-supervisor Viviana Ribeiro for their valuable guidance. This work was partly funded by Sweden's Innovation Agency VINNOVA, through the AM4Life Competence Centre (contract number 2024-03847), which is deeply acknowledged.

Finally, thank you to my family and friends for always being there and supporting me throughout this journey.

Table of Contents

Table of Figures

List of abbreviations

- 3D – Three-dimensional
- BSA–Bovine Serum Albumin
- CO_2 – Carbon dioxide
- DAPI–4',6-diamidino-2-phenylindole
- dECM–Decellularized extracellular matrix
- DMEM – Dulbecco's Modified Eagle Medium
- DMMB – Dimethylmethylene blue
- DNA – Deoxyribonucleic acid
- ECM – Extracellular matrix
- EthD-1 – Ethidium homodimer
- FBS – Fetal Bovine Serum
- G' – Storage Modulus
- G'' – Loss Modulus
- GAGs – Glycosaminoglycans
- H&E – Hematoxylin and Eosin
- h – Hour
- M – $mol.L^{-1}$
- mg – Milligram
- min – Minute
- mL – Millilitre
- mm – Millimeter
- µg – Microgram
- µL – Microliter
- µm – Micrometer
- nm – Nanometer
- PFA – Paraformaldehyde
- PBS– Phosphate Buffered Saline
- PGs – Proteoglycans
- RPM – Rotations per minute
- RCF – Relative centrifugal force
- RT – Room Temperature
- SDS – Sodium Docedyl Sulphated
- UV – Ultraviolet
- ×g – Times gravity
- ºC – Degree Celsius

1.Introduction

1.1. Background-The problem

Organ or tissue transplants between people continue to represent a major medical breakthrough of this century. Nevertheless, the demand for donated organs far outweighs the availability, making the shortage of donor organs one of the most challenging global problems [1]. In 2022, around 52 000 patients across Europe were on transplant waiting lists. According to data from the European Commission, the number of patients awaiting transplantation is categorized by organ type as follows: kidney (16794), liver (6804), heart (2 076), lung (1 815), and other organs [2]. Considering the associated morbidity, mortality, costs, and lack of supportive treatments, xenotransplantation (transplanting organs/tissues between members of different species) has the capacity to address the critical shortage in organ grafts.

Even though xenotransplantation is a potential solution, it is limited by the significant risk of rejection due to foreign tissue immunogenicity [3]. To overcome these immunological barriers and the shortage of donor organs, researchers have turned to alternative approaches such as tissue engineering**.** Instead of depending exclusively on donor organs or xenografts, tissue engineering seeks to develop biological substitutes that can functionally replace damaged organs or tissues. This interdisciplinary field offers a promising solution to address the limitations of traditional transplantation, while also minimizing the risk of immune rejection.

1.1.1. Tissue engineering and regenerative medicine

Tissue engineering was defined as an interdisciplinary field that applies the principles of engineering and the life sciences to the development of biological substitutes that restore, maintain, or improve tissue function [4].

In Tissue Engineering, new materials are designed not only to regenerate damaged tissue but also to coordinate biological responses for clinical use. Typically, viable cells or tissue-inducing compounds are transplanted along with a carrier material to a damaged spot in the body.

The components are chosen based on the tissue to be restored, directing the body to create new functional as shown in **Figure 1**.

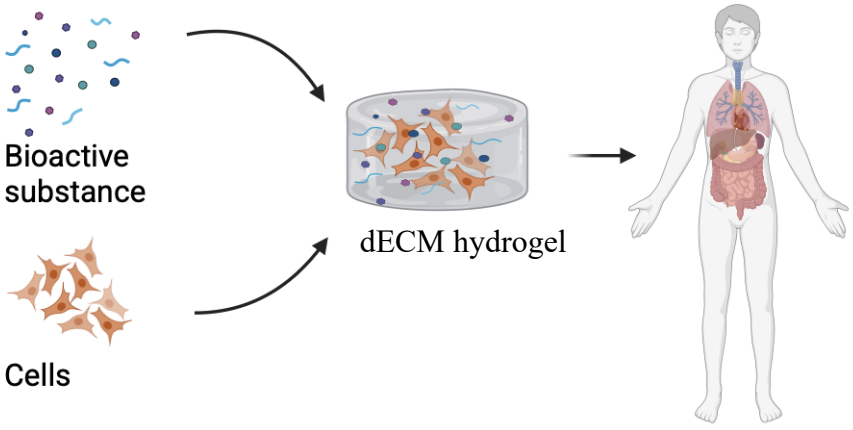

Figure 1 - The principles of tissue engineering involve the delivery of cells and tissue inducing substances with a carrier material for the purpose of restoring lost tissue function. Figure created with BioRender.

The use of scaffolding materials to replicate the tissue extracellular matrix (ECM) offers interesting prospects [5].

1.2. Extracellular matrix

The ECM, as illustrated in **Figure 2**, is an essential component of multicellular organisms, forming a three-dimensional network that surrounds and supports the cells. Far beyond serving as a mere structural scaffold, the ECM plays an important role in regulating essential cellular processes such as growth, migration, differentiation, survival, homeostasis, and morphogenesis [6].

ECM network is composed of various components: collagens, proteoglycans (PGs), glycosaminoglycans (GAGs), elastin, fibronectin, laminins, and other glycoproteins [10]. The composition of ECM and its architecture vary depending on the tissue type, allowing it to fulfill diverse biological functions. Collagen is the most abundant ECM protein, with over 20 genetically distinct types identified [11]. These proteins are characterized by their triple-helix structure, contributing significantly to tissue stability and tensile strength. Collagen type I is particularly prevalent, forming the primary structural framework in many tissues [12,13].

Elastin complements collagen by providing elasticity to tissues like skin, blood vessels, and the bladder, allowing them to stretch and recoil in response to mechanical stress. Together, collagen and elastin define the mechanical properties of tissues, balancing rigidity with flexibility [14,15].

Supporting these structural proteins are glycosaminoglycans, long-chain, negatively charged polymers that imbibe water, giving the ECM its gel-like properties. GAGs are part of proteoglycans, where they are attached to a core protein, forming highly hydrated complexes that help resist compressive forces, regulate water balance, and facilitate cell migration. Hyaluronic acid, a unique non-sulfated GAG, plays a key role in resisting fluid flow and acts as a lubricant in joints, making it especially valuable in cartilage tissue engineering [16–18].

In addition to structural integrity, the ECM also mediates cell adhesion and signaling. Proteins like fibronectin and laminin act as "molecular glue," helping cells attach to the ECM and interact with their surroundings. Fibronectin exists both as a soluble form in blood and an insoluble form in tissues, participating in wound healing and matrix assembly. Laminins, found primarily in basement membranes, are critical for processes such as cell differentiation, migration, and angiogenesis [19–21].

Overall, ECM acts as an active and dynamic regulator of the cellular environment, guiding tissue organization, influencing cell behavior, and maintaining the delicate balance of tissue homeostasis [22].

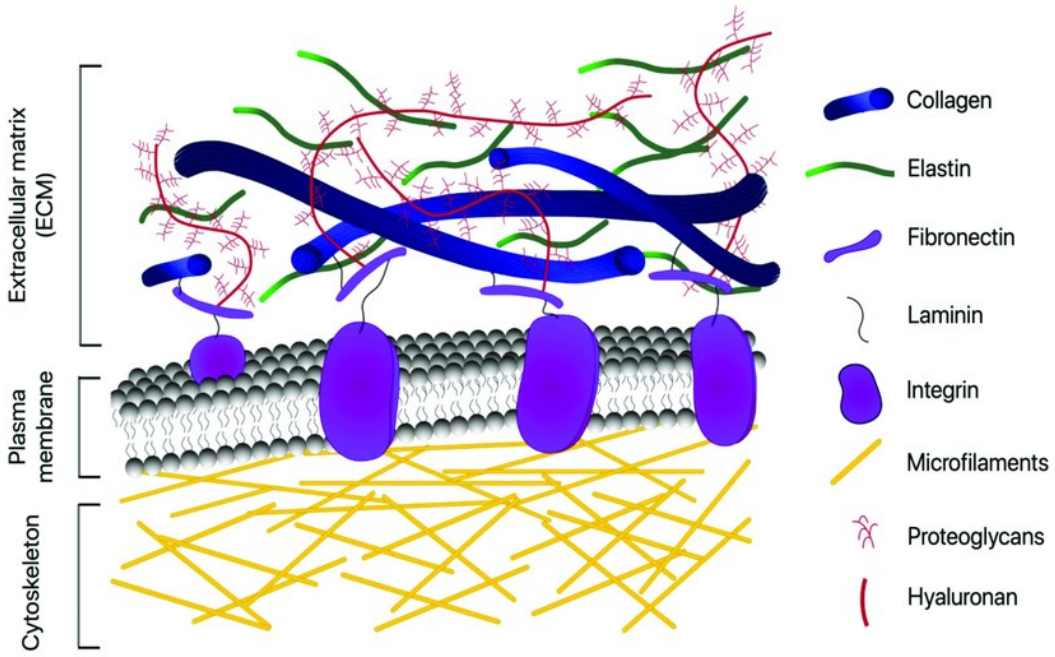

Figure 2 - ECM is made up of many macromolecules that give tissues their strength and shape. It is made up of big structural proteins and polysaccharides that contribute to mechanical characteristics as well as cell signalling and tissue homeostasis. Adapted from [22].

1.3. Decellularized Extracellular Matrix as a Biomaterial

To replicate the complex biochemical and structural cues of native tissues, researchers have increasingly turned to biomaterials that closely mimic the natural ECM. Among these, dECM-based materials have garnered significant interest due to their ability to retain the native tissue's architecture, mechanical properties, and bioactive components such as growth factors and signaling molecules. By removing cellular content while preserving the ECM framework, decellularization provides a biologically relevant scaffold that can support cell adhesion, proliferation, and differentiation [23].

1.3.1. Decellularized ECM

Tissue decellularization consists of removing all the cellular components from the extracellular matrix while maintaining the native ECM structure as demonstrated in **Figure 3.** This can be done by flushing whole organs or by constantly stirring small pieces of tissue [24,25]. The effectiveness of cell removal from a tissue depends on its origin and the physical, chemical, and enzymatic procedures used which can include washes with detergents, enzymes, and buffers [23,24,26].

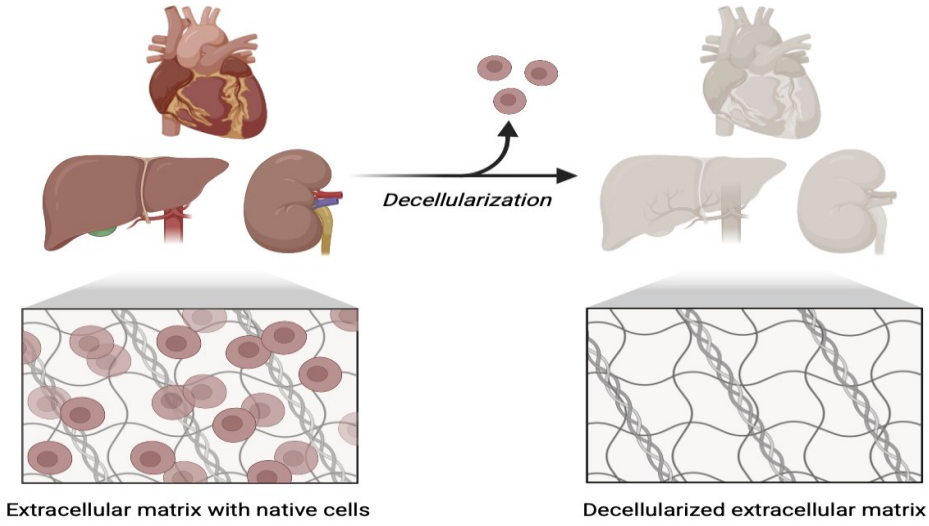

Figure 3 - Schematic of protein composition of extracellular matrix (ECM) before and after decellularization. Figure created with BioRender.

Creating a decellularization protocol is a complicated task. Current decellularization literature identifies numerous potential agents and methods that must be integrated to formulate a decellularization protocol suitable for each type of tissue [23].

1.3.2. Sources of dECM

It is possible to divide the decellularized extracellular matrix into two groups based on their source: human or animal. While human tissue would be optimal in the interest of keeping away from animal diseases spreading and immunogenicity, its availability is insufficient [27,28].

Human tissues and organs can be harvested from cadavers or surgical waste [29]. Xenogeneic tissues are commonly employed in tissue engineering, with a wide range of options available. Although they compensate for the lack of human tissue, they can carry the risk of diseases. Besides, limitations exist due to individual beliefs, such as religious views or a commitment to a vegan or vegetarian way of living.

Among the various sources of animal-derived decellularized extracellular matrix (dECM), porcine tissue stands out as the primary source due to its abundant availability and substantial quantity [30]. From several research papers reviewed, porcine skin is the most commonly used source of dECM, as its composition and functionality closely resemble those of human ECM. In one study, researchers conducted a proteomic analysis of dECM obtained from porcine skin and identified elevated levels of proteins associated with angiogenesis, implying that dECM from porcine skin may enhance wound healing by modulating angiogenesis [31].

1.3.3.Evaluating decellularization

Though the foundational principles of decellularization outlined by *Crapo et al.* (2011) specifically, no visible nuclear material detected by H&E/DAPI, residual dsDNA < ~50 ng per mg dry tissue, and DNA fragment length < ~200 bp are still currently widely referenced, several studies designed to develop definitions of functional responses from decellularized extracellular matrix (dECM) scaffolds have more precisely defined properties that impact the formulation of the quality measure of dECM [23].

However, recent studies showed that the 50ng/mg threshold can serve as an appropriate guideline but is not an absolute amount that means a scaffold is immunologically safe, and methods of quantification may suffer from artifacts impacting results, such as loss of smaller DNA fragments during extraction, causing problems in quantifying residual cellular material [28,32].

1.4. 3D Printing and Bioprinting in Tissue Engineering

In recent years, additive manufacturing technologies, especially 3D printing and bioprinting, have transformed the landscape of tissue engineering [33]. Unlike conventional fabrication

methods, 3D printing is a layer-by-layer process to fabricate highly defined, patient-specific architectures directly from digital models.

This spatial control enables the creation of constructs with complex architectures, tailored mechanical properties, and controlled gradients of cells and signaling molecules, critical characteristics for replicating the native tissue microenvironment [34]. Importantly, bioprinting incorporates cells directly during fabrication, bypassing the need for post-fabrication seeding and enhancing initial cell distribution and viability.

Among the available bioprinting modalities, such as inkjet, laser-assisted, and extrusion-based, the last one is the most widely used for tissue engineering due to its ability to process highly viscous bioinks, including those derived from decellularized extracellular matrix [12,35]. This approach is compatible with high cell densities and diverse material formulations, although it can subject cells to shear stress during extrusion.

1.4.1. Extrusion-based bioprinting

Extrusion-based bioprinting is the most prevalent technique utilized in 3D bioprinting, in which a bioink is inserted into a cartridge and extruded with the assistance of a piston, screw, or pressure, as shown in **Figure 4**. This is attributed to the method providing a straightforward and economical way to dispense the bioink. It can extrude bioinks across various viscosities, concentrations, and cell densities. This approach enables a simple printing process of filaments layer-by-layer that continually extrudes the bioink. The constructs are produced by having the platform shift along the y-z axis or by the syringe with the attached nozzle progressing in the z-axis, while simultaneously the nozzle moves along the x-axis. The established printing speed and selection of nozzle diameter facilitate the rapid printing of large-scale constructs within a short timeframe [36].

The primary drawbacks are linked to the shear stress induced by the pressure from the nozzle walls during extrusion and the high pressure, which restricts cell viability when printing bioinks that contain live cells. Cell viability may also be compromised when printing larger constructs, which necessitates additional time, as cells encounter risks of dehydration and nutrient shortage [12,34,37]. Nonetheless, extrusion-based bioprinting is widely used to print an

array of bioinks including cell-aggregate-based, cell-laden bioinks, and components of decellularized matrix that may not be printable through alternative methods.

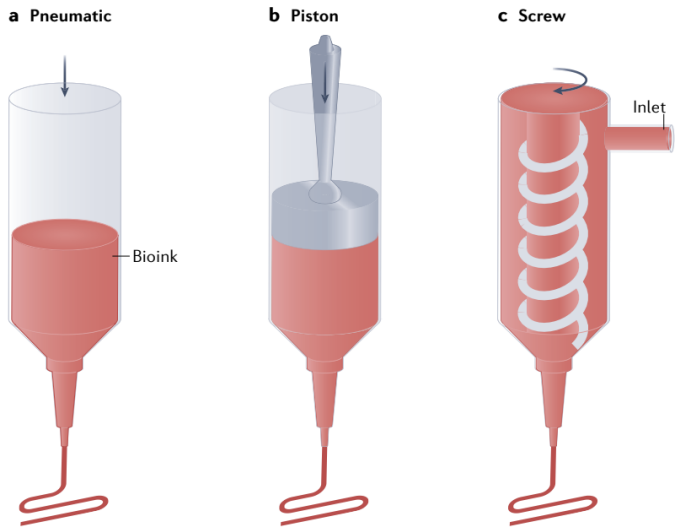

Figure 4 - Extrusion bioprinting methods. Adapted from [37].

There are many factors to consider while choosing an appropriate bioink. First, biocompatibility and cell viability must be evaluated. The bioink should be non-toxic and non-inflammatory to cells, while also promoting cell adhesion, proliferation, and differentiation. Before printing, it's important to do preliminary experiments to determine which bioinks are best for cell viability.

1.4.2.Literature Examples of Bioprinting with dECM and Other Bioinks

Among all the techniques available for bioprinting, extrusion-based bioprinting has become one of the most widely adopted due to its versatility, cost-effectiveness, and compatibility with a wide range of bioinks, including hydrogels derived from decellularized extracellular matrix (dECM) [28].

By definition, a bioink consists of a combination of a biomaterial, such as a hydrogel, as used in this work, and living cells. Therefore, we need to ensure these inks provide the structural

support and environment necessary for cells to survive, proliferate, and form complex tissues that mimic native ones [12].

There are various types of bioinks used in bioprinting. Synthetic bioinks offer tunable mechanical properties and reproducibility but lack bioactivity, whereas other naturally derived hydrogels such as collagen, fibrin, hyaluronic acid provide some biological cues but cannot fully recapitulate the complexity of native ECM.

Bioinks, such as alginate, gelatin, and synthetic polymers, offered ease of processing but may lack the biochemical complexity of native ECM, resulting in limited cell–matrix interactions and suboptimal tissue development. For example, alginate is bioinert, preventing effective cell adhesion and remodeling, which constrains differentiation potential [12]. In contrast**,** dECM-based bioinks retain structural proteins, glycosaminoglycans, and tissue-specific cues that promote cell viability, and functional tissue remodeling [38,39].

In a seminal research work, *Pati et al.* (2014) showed the use of tissue-specific dECM bioinks derived from adipose, cartilage, and heart tissue for printing cell-laden constructs [12]. These constructs showed high cell viability and expressed tissue-specific genes, underscoring the importance of matching ECM origin to the intended tissue application. Similarly, [6] developed a tendon-derived dECM hydrogel bioink with gelation kinetics tailored for extrusion without additional crosslinkers. This approach allowed support-structure-free printing while preserving cytocompatibility and enabling encapsulated cells to adopt lineage-specific morphologies.

Despite these advantages, dECM hydrogels typically present limitations such as mechanical strength and print fidelity, largely due to their reduced viscosity and slow gelation after solubilization [38]. Strategies to overcome these issues include combining with other polymers, for example gelatin, alginate to improve rheology and mechanical properties, or using hybrid printing approaches where a thermoplastic polymer, for example polycaprolactone (PCL), provides structural support while the dECM hydrogel delivers bioactivity. However, these modifications may introduce heterogeneity or biocompatibility concerns [6]. The ongoing challenge is to balance printability, mechanical stability, and biofunctionality to produce constructs that both survive the fabrication process and foster appropriate cellular responses in vitro and in vivo [39].

In this context, using dECM bioinks offers significant potential for the fabrication of biomimetic tissue microenvironments. Nevertheless, achieving an optimal balance between structural fidelity and biological functionality remains a key challenge. The rheological behavior and gelation kinetics of dECM hydrogels must be carefully tailored to ensure both high-quality printing and the preservation of cellular viability.

1.5. Previous research

In our research group, a protocol for extracting dECM from porcine skin and producing hydrogels was previously developed [40]. Three pre-gel formulations were tested: 1, 2.5, and 5 $mg \cdot mL^{-1}$. Gelation times at 37 °C were 36, 22.5, and 6.8 minutes, respectively. All formulations exhibited shear-thinning behavior suitable for extrusion printing, with higher concentrations showing greater viscosity and more homogeneous prints. The 2.5 and 5 $mg \cdot mL^{-1}$ hydrogels were better for printing, with 5 $mg \cdot mL^{-1}$ providing the best shape fidelity [40,41].

Cell studies showed that softer gels allowed cell infiltration and network formation, whereas denser gels restricted migration. In denser gels, fibroblasts remained on the surface, proliferated less, and were rounded; in softer gels, they spread and elongated. These results indicated that 2.5 $mg \cdot mL^{-1}$ provided an optimal balance for printing and assessing the effect of dECM concentration on cellular behavior, and this concentration was used in all subsequent experiments.

1.6. Aim of the Thesis

This thesis focuses on developing a bioprinting protocol that optimizes cell viability and improves shape fidelity using bioinks derived from decellularized extracellular matrix of porcine skin, for applications in 3D bioprinting and tissue engineering.

1.7. Work Plan

In this study, porcine skin was decellularized to obtain an extracellular matrix following a previously established protocol [40]. The resulting ECM was then used to produce a hydrogel.

To evaluate the effectiveness of the decellularization process, we quantified the remaining DNA, glycosaminoglycans (GAGs), collagen, and elastin content.

Next, we carried out rheological measurements of the gel to assess its mechanical properties. Simultaneously, we began familiarizing ourselves with the bioprinter, experimenting with different printing patterns and needle tips to determine the most suitable settings for working with the gel.

Subsequently, we proceeded to bioprint the gel within the cells, to develop and optimize a bioprinting protocol that supports cell viability and proliferation. Then, to evaluate this, we used optical and confocal microscopy techniques.

2. Materials and methods

2.1. Materials

Porcine skin tissue was purchased from a local supermarket (City Gross, Uppsala, Sweden) and preserved at −20°C before subsequent utilization. Pepsin from porcine gastric mucosa, Papain from Papaya Latex, Sodium Dodecyl Sulfate, Triton X-100, Phosphate Buffer Saline, Dimethyl Methylene Blue, L-cysteine, and Chondroitin Sulfate were purchased from Sigma-Aldrich (Solna, Sweden). Glacial Acetic Acid was purchased from Merck (Solna, Sweden). For all the experiments, ultrapure MilliQ water (Millipore) was used.

2.2. Decellularization of porcine skin tissue

For the decellularization process of the tissue, a previously established protocol was followed, as described by *Palierse et al*. (2025) [40], which was inspired by and modified from published protocols *Pati et al.* (2014) [12]. The subcutaneous fat was removed from the porcine skin tissue. Then the remaining dermal tissue was cut into cubes, which were homogenized in a lab-grade grinder (Mill SM-3, Hsiang Tai) until a paste was formed and subsequently subjected to two 30-minute acetone treatments with continuous stirring to eliminate any traces of lipids. A ratio of approximately 10 milliliters of solvent per initial gram of tissue was utilized for every stage of the decellularization procedure.

Next, the minced tissue was washed with 1% Sodium Dodecyl Sulfate (SDS) in PBS for 42 hours. Afterwards, the tissue was treated with 1% Triton X-100 for 30 minutes, followed by washing in PBS for 2 days with renewal of the solution twice daily. The tissue was then sterilized using a mixture of 1% Acetic Acid and 3% Hydrogen Peroxide for 2 hours. Two washes with PBS followed this for 15 minutes, and then two washes with ultrapure MilliQ water for 15 minutes.

The resulting solid material was then freeze-dried for 24 h. Following freeze-drying, the material was ground and rinsed twice with acetone for 30 minutes each. To make sure the acetone was removed, it was then rinsed with MilliQ water two times.

dECM tissue was frozen in liquid nitrogen and lyophilized with a FreeZone Plus lyophilizer (Labconco, US) and stored at −20°C before further use.

2.3. Evaluation of decellularization: Biochemical characterization of dECM

Biochemical assays were used to detect the presence of the major skin components in dECM, such as collagen, elastin, and sulfated glycosaminoglycans (GAGs), as well as DNA content. All results were compared with those obtained from a previous batch described in *Paliers*e *et al.* (2025*)* [40], to evaluate the efficacy of the optimized decellularization protocol. For all the tests, the absorbance or fluorescence of the solutions was measured using a Tecan Infinite M200 plate reader. All tests were performed in triplicate.

2.3.1. Collagen Quantification

For collagen quantification, a Sircol Soluble Collagen Assay kit from Biocolor. The day before the assay, dECM was dissolved with pepsin in 0.5 M acetic acid at 4 °C for 16 hours and then assessed according to the kit instructions. The absorbance was measured at 556 nm.

2.3.2. Elastin Quantification

Elastin contents were measured using the Fastin Elastin Assay from Biocolor, according to the manufacturer's instructions and the absorbance were measured at 513 nm.

2.3.3 GAGs and DNA Quantification

For GAGs and DNA quantification, dECM was first digested in a papain solution (125 $\mu g.ml^{-1}$ papain in 0.1 M sodium phosphate with 5 mM Na_2-EDTA and 5 mM cysteine-HCl at pH 6.5), at a concentration of 50 $mg.mL^{-1}$ for 16 h at 60 °C with stirring 300 rpm. The

solution was then centrifuged 3 min at 10 000 ×g using a Centrifuge 5417 C Eppendorf, and the supernatant was filtered with a 0.22 µm filter.

GAG content was quantified using the dimethylmethylene blue (DMMB) assay. The DMMB reagent was prepared by dissolving 3.2 mg of DMMB, 0.608 g of glycine, and 0.32 g of NaCl in 19 mL of 0.1 M acetic acid. Then, 100 mL of MilliQ water was added, and the solution was diluted to a final volume of 200 mL with additional MilliQ water. The reagent was protected from light. A standard curve consisting of chondroitin sulfate (0 − 250 µg/mL) in MilliQ water was used. 20 µL of the standards and samples were loaded in triplicate into a 96-well plate, followed by 200 µL of the DMMB solution. The plate was shaken for 1 minute in the dark and then immediately measured for absorbance at 525 nm.

DNA quantification was measured using Quant-iT PicoGreen dsDNA Assay kit from Invitrogen's according to the manufacturer's instructions.

2.4. Preparation of dECM pre-gel and gels

dECM pre-gels were prepared following the enzymatic digestion of freeze-dried dECM at a concentration of 5 $mg.mL^{-1}$, using 2 mg of pepsin (P6887, Sigma Aldrich) per 100 mg dECM at 4 °C in a 0.5 M acetic acid solution during the night. The protocol was adapted from [42].

Following solubilization, the pH was adjusted to 7.2−7.4 by employing sodium hydroxide at 10 and 1 $mol.L^{-1}$, along with acetic acid at 1 and 0.5 $mol.L^{-1}$, while maintaining the temperature under 10 °C. The solution was mixed for 1 hour at 4 °C to allow the pH to stabilize. The pH was adjusted again if needed. The mixture was centrifuged at 1000 rcf for 5 minutes to eliminate any undissolved lipid fragments. dECM pre-gels were kept at 4 °C in the fridge and used or studied within a week. To prepare a pre-gel at 2.5 $mg.mL^{-1}$, the concentrated pre-gels stock was diluted using PBS. The dECM hydrogels were obtained after 1 – 2h incubation of pre-gels at 37 °C. Only pre-gels and hydrogels at 2.5 $mg.mL^{-1}$ were used in this study.

2.5. Rheological Characterization

Rheological measurements were performed using a Discovery HR-10 Rheometer (TA Instruments, USA), equipped with a 20 mm diameter steel parallel plate as the top geometry and a steel Peltier plate as the bottom geometry. Viscosity of the hydrogels was evaluated by plotting viscosity (Pa.s) versus shear rate (1/s) in **Section 3.3. Rheological measurements. – Results.** Before each measurement, any excess sample was carefully removed using a paper towel.

2.6. dECM Gel Preparation within the syringe

The pre-gel was transferred to a 1 mL plastic syringe (Fisher Scientific) and incubated in an oven at 37 °C for 1 hour. During initial printing attempts, extrusion was unsuccessful due to the presence of air bubbles within the ink. To address this, air bubbles were manually removed before incubation; however, some bubbles persisted and continued to obstruct extrusion. To resolve this, before the incubation step, the syringes were centrifuged using a Megafuge 8 centrifuge from Thermo Scientific at 1000 rcf for 5 minutes. This centrifugation step effectively eliminated the remaining air bubbles, resulting in consistent and unobstructed extrusion during the printing.

2.7. Printing Setup

An open-source bioprinter based on the E3D motion system was used for extrusion-based printing [37]. All digital models were created using SolidWorks software, then exported as STL files. The models were sliced using Simplify3D and further processed in Python to generate G-code instructions for the printer.

2.8. Printing Conditions and Testing

Gels at 2.5 mg.mL^{-1} were tested extruded using different sizes of needle tips through an 18G, 22G, 23G, 25G, and 30G syringe with an inner diameter of 0.44 mm, 0.41 mm, 0.34 mm, 0.25 mm, and 0.15 mm, respectively. Printing occurred at room temperature, with a 600 mm.min^{-1} speed.

To assess print resolution and spreading, a two-layer cube was printed on polystyrene petri dishes (Sigma Aldrich), as well as 6 well and 24 well tissue culture plates (Avantor, VWR). Although more than two layers were also tested, the structures collapsed beyond this point.

Finally, to test for the layer stacking, a square plate with the dimensions 15 x 15 mm^2 was printed in a polystyrene petri dish with the following parameters: 2 layers, infill grid 40%.

Pictures were captured using Dinocapture 3.0 software on a digital microscope (Dino-Lite Europe, Almere, The Netherlands) immediately after printing. The photos were analyzed using ImageJ software later.

2.9. In vitro cell culture

L929 murine fibroblasts (ECACC 85011425) were cultured in Dulbecco modified eagle medium (DMEM) with high glucose and L-glutamine (Gibco 11965092) supplemented with 10% Fetal Bovine Serum (FBS) (Gibco 11560636) and 1% Penicillin/Streptomycin (Sigma-Aldrich, P4333) in a 37 °C, 5 % (v/v) CO_2 environment. The cells were detached from culture flasks, using TrypLE (Gibco, 11528856) for 4 minutes at 37 °C and adding pre-warm medium, then the cells from the flask were transferred to a Falcon tube to centrifuge at 125 g for 7 minutes. The cells were passaged twice a week, when 70-90% confluence was reached.

2.10. Bioprinting Protocol with cells

Initially, the needle tip selected for each experiment, the syringe cap, and the female adaptor were sterilized by immersion in 70% ethanol for 10 minutes. Subsequently, 2 mL of the pre-gel stock solution at 5 mg/mL was exposed to UV light for 10 minutes for sterilization. Following sterilization, the pre-gel stock solution at 5 mg/mL was mixed with 1X PBS at a ratio 1:1 (named this as pre-gel*) and incubated at 37 °C for 1 hour. During this period, cells were prepared for encapsulation.

After centrifugation, the cells were counted, typically yielding a concentration of 5×10^5 cells/mL. Therefore, they were concentrated to reach a concentration of 1×10^6 cells/mL. The resulting cell pellet was then mixed with the pre-gel. The cell-gel suspension was carefully transferred into a sterile syringe using a female adaptor to ensure homogeneous mixing and to minimize the presence of air bubbles, which could otherwise clog the needle tip during the bioprinting process. The loaded syringe was incubated at 37 °C in 4% CO_2. Bioprinting was performed in a 24-well plate. After 5 minutes, we attempted to add 100 µL of culture medium, but this unfortunately disrupted the printed structure. Therefore, we instead added 50 µL of culture medium to each well to provide sufficient nutrients to support cell viability and growth within the hydrogel matrix.

In the initial stages of the study, we attempted to mix the pre-gel solution with 1X PBS and add the cells simultaneously, followed by incubation for 1 hour at 37 °C with 5% CO_2. In the initial stages of the study, we also attempted to mix the pre-gel* with cell culture medium. However, after the incubation period (and even with extended time), gelation was not achieved. Alternatively, we tested resuspending the cell pellet in culture medium before mixing it with the gel, as we were uncertain whether the cells would survive 1 hour without nutrients. However, even with this modification, gelation was not observed within the expected time frame, especially when compared to the gel formed in the oven. **Figure 5** presents an overview of the protocols we tested. For the further experiments, we followed Protocol b).

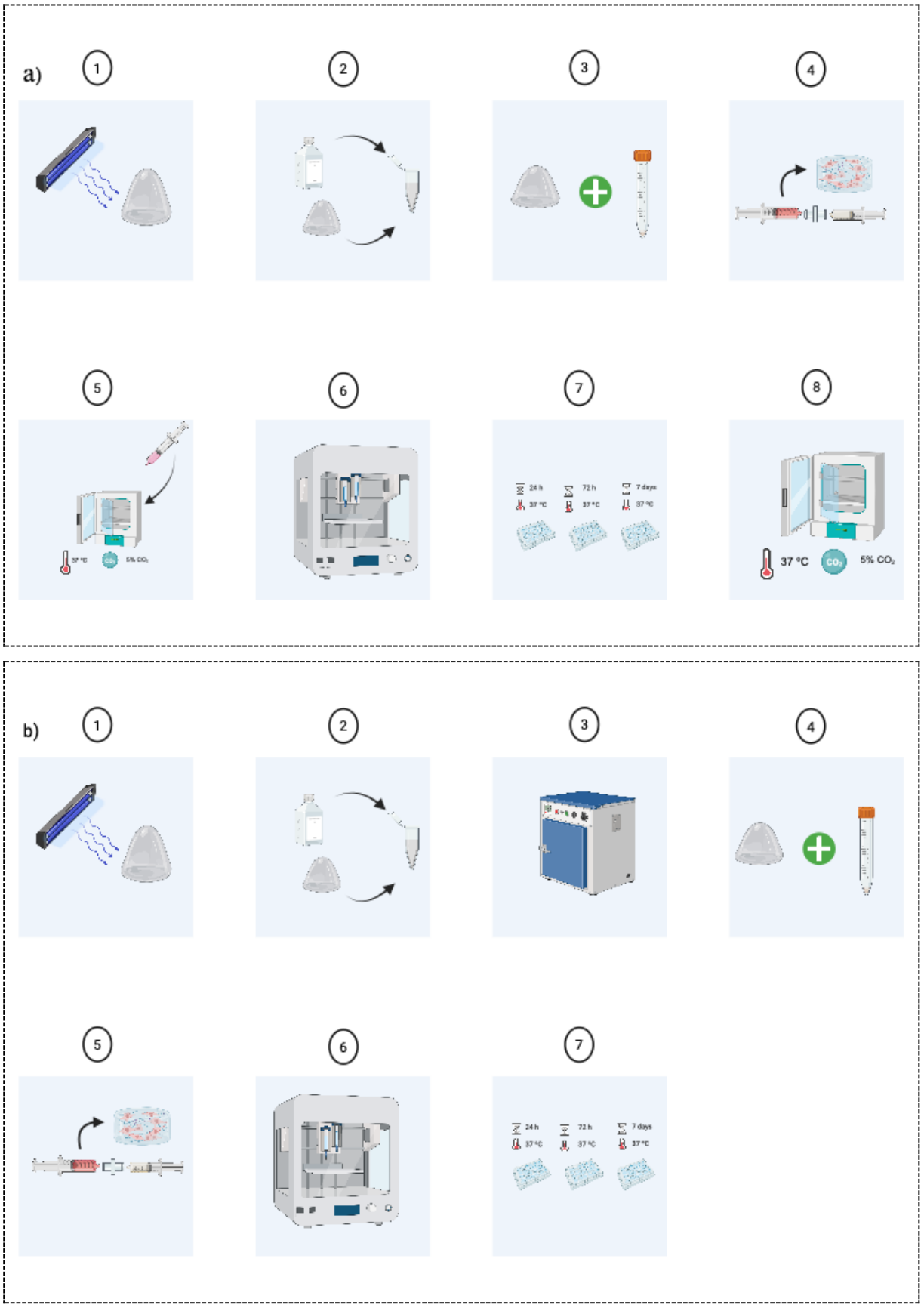

Figure 5 - Overview of the protocol flow: a) the gel was made in the incubator at 37 °C with 5% CO_2 and b) the gel was made in the oven at 37 °C. Figure created with BioRender.

2.11. Immunostaining

To perform the fixation, samples were covered with 4% PFA in PBS (PFA, Sigma Aldrich) for 10 minutes at room temperature and washed with PBS three times. After that to permeabilize the samples were covered with 0.1 % Triton X in PBS for 10 minutes and washed three times with PBS. For blocking, the samples were incubated with 2% BSA in PBS for 1 hour at room temperature.

To carry out staining, the samples were incubated with Actin staining 488 (2 drops / mL) and DAPI (5 µg/mL) for 1 hour at room temperature in the dark. Lastly, they were washed in PBS and stored at 4°C covered in PBS before imaging.

2.12. Confocal fluorescence microscopy imaging

Imaging using a confocal fluorescence microscope was conducted with a SP8 confocal laser scanning microscope (Leica), utilizing a 10 × air objective. Images were captured at a resolution of 1024 × 1024 pixels with a speed of 400 lines per second.

2.13. Data Treatment and Graphical Analysis

The collected data were initially processed and organized using Microsoft Excel. Graphs and data visualizations were subsequently generated using Python (version 3.12) in the Spyder IDE, included in the Anaconda distribution.

3. Results and discussion

3.1. Tissue Processing and Evaluation of Decellularization

Different from other studies focused on the dermal layer, here we aimed to use the whole skin tissue without isolating the three different layers, epidermis, dermis and hypodermis [43,44]. Visual inspection of the tissue showed that the skin went from having a pale pinkish-white tone to completely white after decellularization, as shown in **Figure 6**.

Figure 6 - Representative native and decellularized skin tissue. a) Representation of skin section before decellularization. b) Representation of skin sections after decellularization. c) Appearance of decellularized skin after freeze-drying and milling. d) dECM gel after 1h-2h incubation in the oven at 37°C.

The concentrations of the main ECM components, such as collagen, elastin, and GAGs, in µg per mg of dry tissue or ECM, as shown in **Figure 7,**indicate the effectiveness of lipid removal and were compared to the previous batch prepared by *Palierse et al.* (2025) [40].

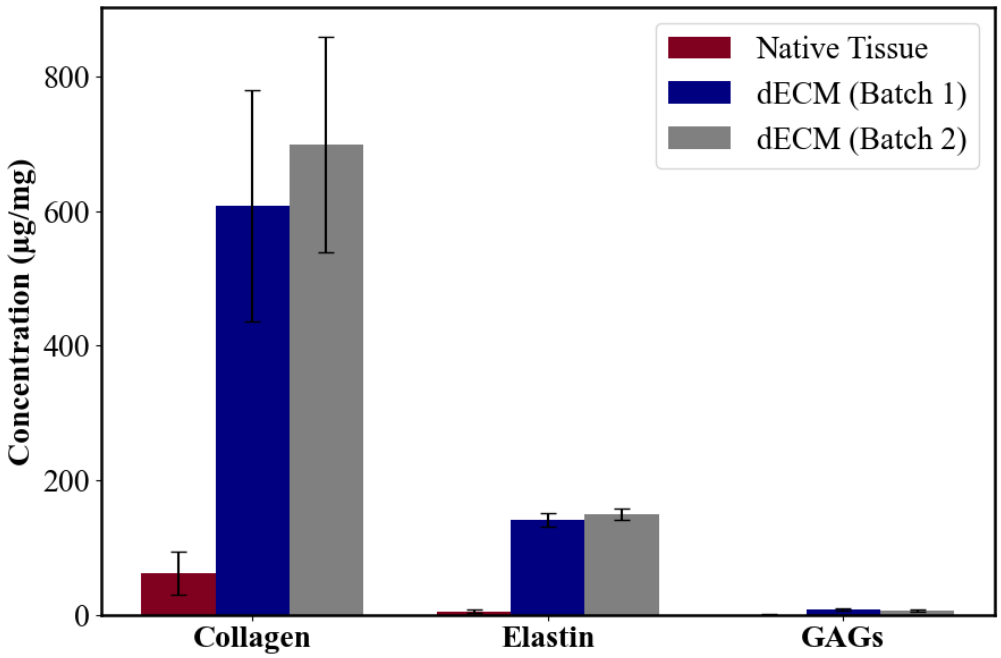

Figure 7 - Biochemical analysis of decellularized tissues. ECM component concentrations are presented in µg per mg of dry tissue or dry dECM. The dECM (batch 1) shows results from *Palierse et al.* (2025) and dECM (batch 2) graph shows results from the current decellularization process used in this thesis.

The composition of the decellularized extracellular matrix obtained in this study was compared to a previous batch reported by [40]. In the current study, the quantified amounts of collagen, elastin, and GAGs were 699 $\mu g \cdot mg^{-1}$, 199 $\mu g \cdot mg^{-1}$, and 6.844 $\mu g \cdot mg^{-1}$, respectively, compared to 608 $\mu g \cdot mg^{-1}$, 142 $\mu g \cdot mg^{-1}$, and 9.1 $\mu g \cdot mg^{-1}$ measured in the previous batch.

The similarity in the values obtained across both preparations confirms the reproducibility of the decellularization protocol, as well as the consistency of the biochemical quantification methods. Minor variations were observed such as a modest increase in collagen and GAG content and a slight decrease in elastin, this can be attributed to biological variability between part of the tissue or small operational differences, which are expected when working with biological materials. Nonetheless, the overall biochemical profile remained consistent.

This reproducibility is important for applications in tissue engineering and biofabrication, since it ensures that the material properties of dECM-based bioinks exhibit minimal batch-to-batch variation. As a result, material properties remain stable, supporting predictable cell behavior, consistent scaffold performance, and scalability for future applications [45].

The preservation of the ECM components after decellularization can be assessed by presenting the latter results in percentage of the initial quantities in the native tissue used for decellularization, as shown in **Figure 8.**

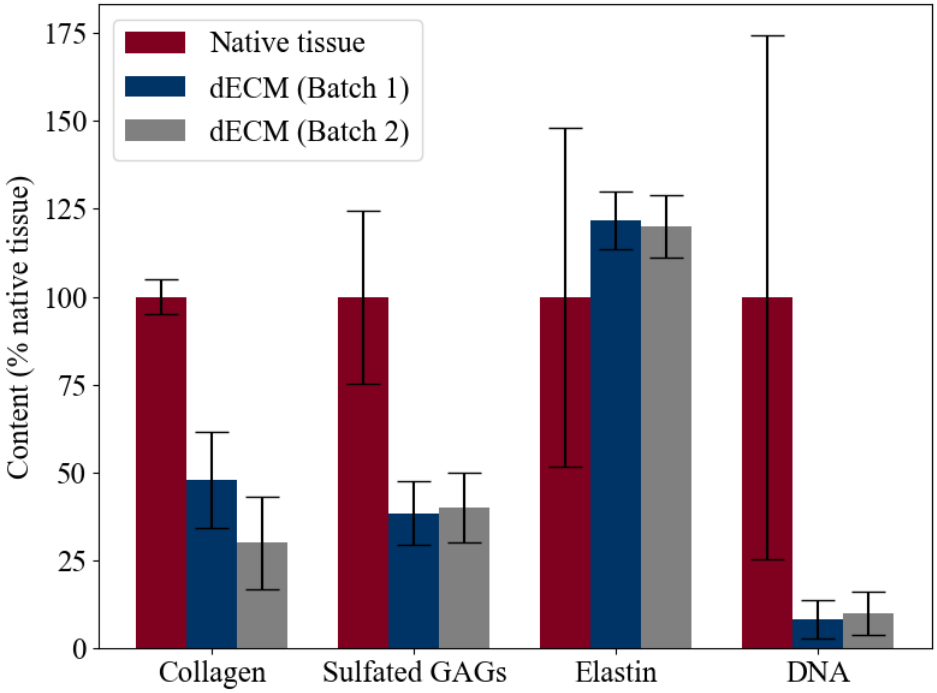

Figure 8 - Biochemical analysis of decellularized tissues. Maintenance of ECM components (collagen, sulfated GAGs, elastin) and DNA after decellularization. The dECM (batch 1) shows results from *Palierse et al.* (2025) [40], and dECM (batch 2) graph shows results from the current decellularization process used in this thesis.

The removal of DNA is crucial for efficient decellularization. We observed a reduction of DNA in dECM compared to native tissue, with ~12% of DNA present after decellularization for batch 1 and ~14% of DNA present after decellularization for batch 2.

These results indicate that the decellularization methods effectively reduce DNA content relative to native tissue, and that the current process demonstrates good reproducibility and

consistent DNA clearance, which are essential for minimizing immunogenicity in tissue engineering applications.

3.2. Printing tests with dECM hydrogel

The printability of the dECM hydrogels at 2.5 mg.mL^{-1} concentration was studied with extrusion-based 3D printing. In a first study, to determine how the needle gauge affected the ink's extrusion performance, several needle sizes 18G (0.44 mm), 22G (0.41 mm), 23G (0.34 mm), 25G (0.25 mm), and 30G (0.15 mm) were examined, as illustrated in **Figure 9.**

Needle tip					
Gauge	18G	22G	23G	25G	30G
ID (mm)	0.44	0.41	0.34	0.25	0.15
Extrude or not	Yes	Yes	Yes	Yes	No

Figure 9 - Comparison of Needle Tips by Gauge, Dimensions, and Extrusion Capability.

The results showed successful extrusion through all needle tips except the 30G needle. The failure of extrusion through the 30G needle, which has the smallest inner diameter, is due to the increased flow resistance associated with the narrow tip. This suggests that the rheological properties, such as viscosity and potential yield stress exceed the force that can be manually applied or delivered by the extrusion system used, thereby preventing the initiation and maintenance of flow through such a small diameter [46].

To evaluate printability, the same cube pattern was printed using dECM gel at 2.5 mg·mL^{-1} concentration at a speed of 600 mm·min^{-1} on a polystyrene Petri dish, a substrate commonly used in cell culture. According to [40], this speed resulted in more homogeneous prints and was therefore selected for all experiments in this thesis. For the printing test, a gel-filled syringe

was used to print a cube design (15 mm × 15 mm with 40% infill and 2 layers) using needle tips of varying sizes: 18G, 22G, 23G, and 25G as shown in **Figure 10.**

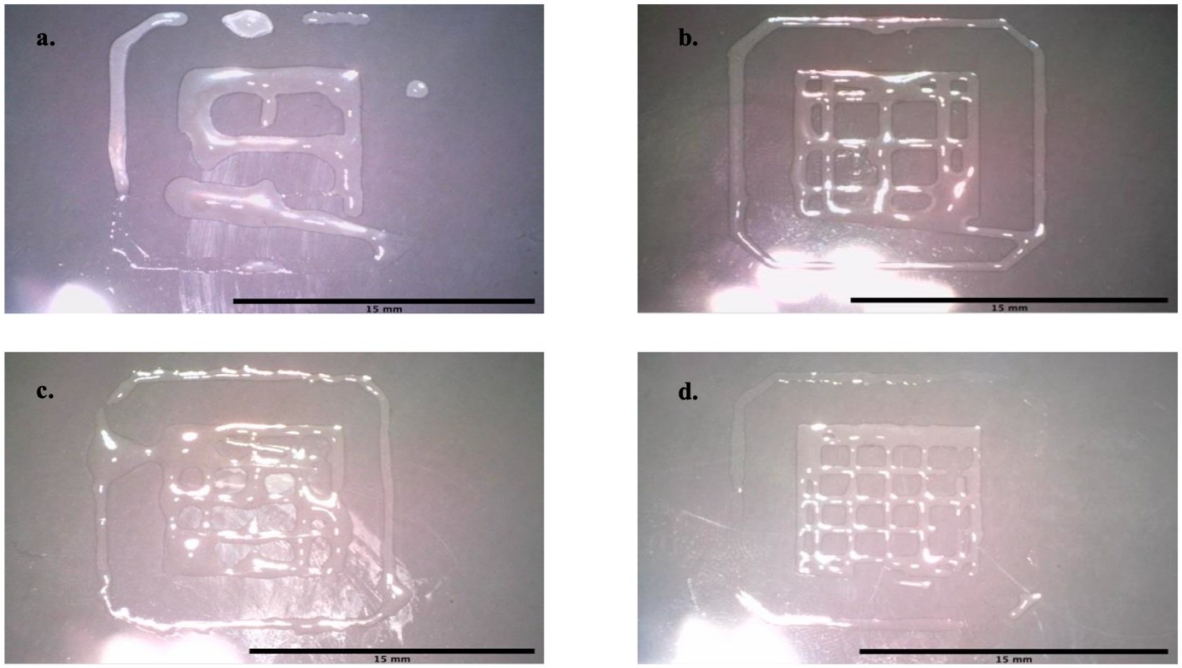

Figure 10 - Printability of dECM bioinks on plastic substrate. Pictures taken directly after printing with gel at a 2.5 mg.mL^{-1} a. 18G; b.22G; c.23G and d.25G.

To evaluate the influence of needle gauge on filament formation, the filament diameters extruded through four different needle sizes (18G, 22G, 23G, and 25G). Post-print images were captured using a digital microscope, and filament thickness was measured at eight distinct points. As shown in **Figure 11**, all conditions yielded filaments with diameters in the range of ~0.010 mm, but notable differences were observed depending on the gauge.

The 23G needle produced the thickest filaments, followed by 18G and 25G, while the 22G needle resulted in the smallest average diameter. Despite the 18G needle having a larger internal diameter, the resulting filament was slightly thinner than that from the 23G, potentially due to backpressure effects or differences in flow resistance. The 25G needle, while more restrictive, produced filaments comparable in thickness to the 18G, but with slightly more variation.

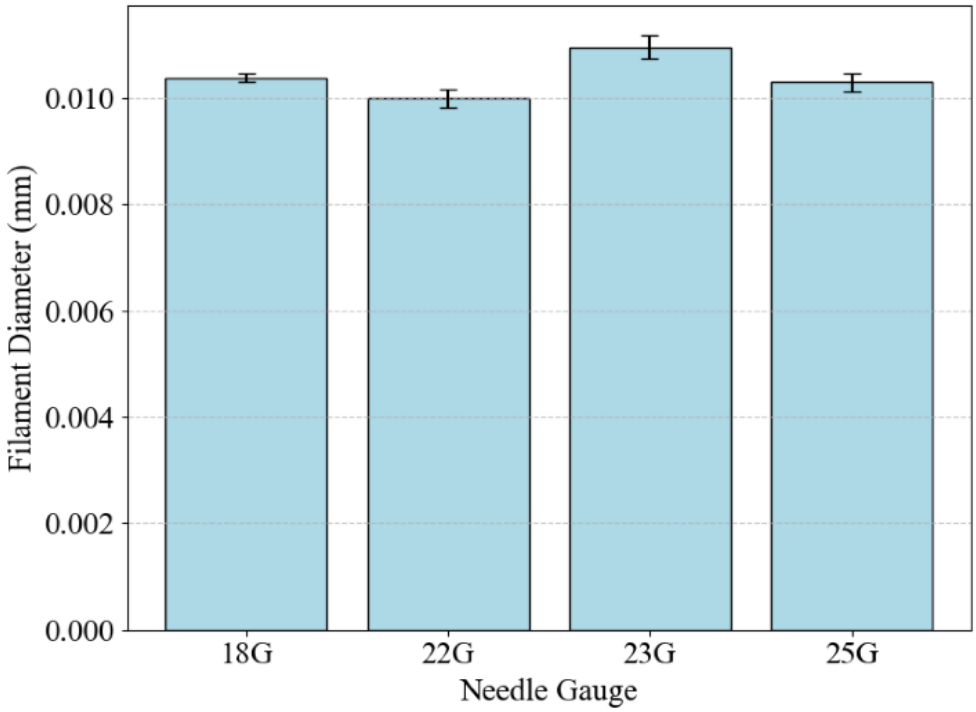

Figure 11 - Filament diameter measured using different needle tip gauges (18G, 22G, 23G and 25 G).

Considering both filament consistency and average diameter, the 23G needle appears optimal for applications requiring high print fidelity and extrusion. Its ability to form relatively thicker and more consistent filaments suggests a good balance between extrudability and structural integrity, which is essential for maintaining filament shape and avoiding nozzle clogging during bioprinting or similar processes. Therefore, a 23G needle was used in all subsequent experiments involving cell encapsulation within the gel.

3.3. Rheological measurements

After we prepared and printed the gels without cells, we moved on to print the cells-containing hydrogels prepared using cell media. We first thought that some constituents in the media could affect the rheological properties of the gel. To check this, we compared the rheological behavior of the hydrogels prepared with PBS to those prepared using culture medium, as detailed in **2.9. In vitro cell culture**. We took FBS out of the media, since its high protein content could raise the viscosity and density of the solution [47].

Figure 12 shows the low viscosity of the hydrogels, which decreases with decreasing concentration. At $10s^{-1}$ shear rate, dECM hydrogels have viscosity below than 0.05 Pa.s.

All hydrogels possess shear-thinning properties with lower viscosity at higher shear rate. The range of viscosity of dECM gel, combined with their shear thinning properties, make them suitable for injectability or extrudability of gels. According to [33] the use of materials with a viscosity range between 30 mPa/s to > 6×10^7 mPa/s have been shown to be compatible with extrusion based bioprinting, with higher-viscosity materials frequently providing structural support for the printed construct and lower-viscosity materials providing a suitable environment to ensure cells remain alive and functional [33].

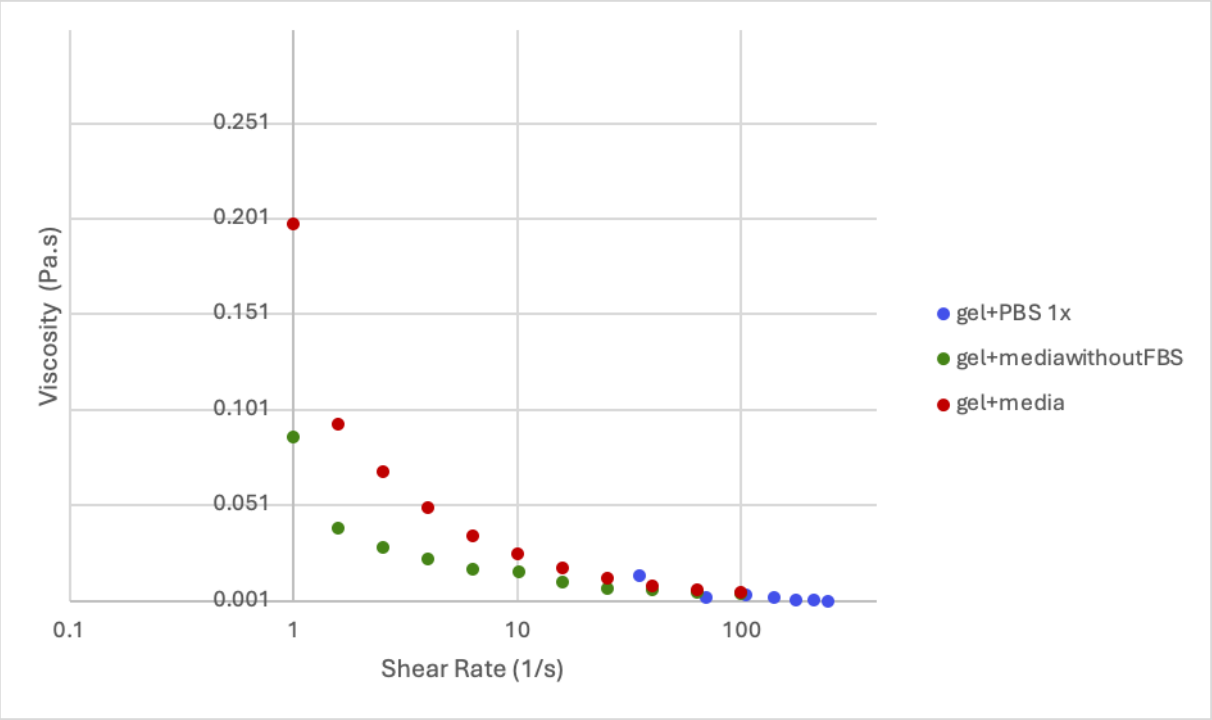

Figure 12 - Viscosity behavior of gels under increasing shear rate for all the conditions.

From the three conditions, all possess shear thinning properties, which means the constituents of the culture medium did not have a significant impact on gel rheology. Further investigation showed that the differences in viscosity were due to varying humidity levels between the incubator and the oven. The humid conditions in the incubator kept the gels from fully drying out, resulting in lower viscosity compared to gels made in dry oven conditions.

3.4. Protocol development

At this point in the study, we encountered challenges in establishing an optimized protocol. Initially, the hydrogel was prepared and simultaneously resuspended on the cell pellet, followed by incubation at 37 °C with 4% CO_2. However, the gel failed to solidify properly, even after prolonged incubation. To address this, we modified the protocol by omitting FBS from the culture medium during the initial steps and adding it only after the printing process. Despite this adjustment, the gel still did not exhibit the expected consistency after 1 hour of incubation. Subsequently, we prepared the gel by incubating it at 37 °C in a dry oven (i.e., without humidity) before resuspension and printing. This approach yielded a more viscous gel, likely due to the absence of humidity, which appeared to enhance gelation.

In **Figure 13** ,we can see the gel made for a period between 1h-2h, on the left side made in the oven more viscous, and on the right side, made in the incubator, with more water content, especially surrounding the gel.

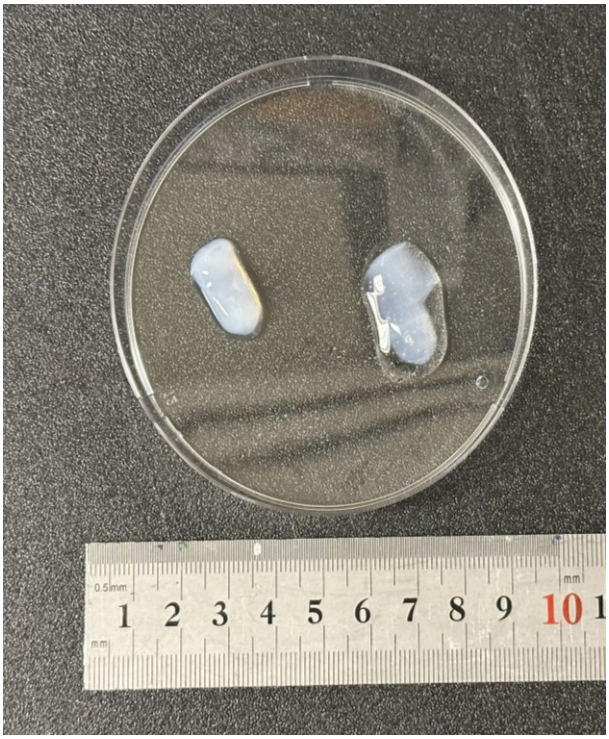

Figure 13 - Gel prepared in the oven (on the left side) and gel prepared in the incubator (on the right side).

In **Section: 2.10. Bioprinting Protocol with cells,** we can see with detail the protocol chosen for the rest of the study.

3.5. Cell culture on dECM hydrogels

Cells were encapsulated within dECM hydrogels and extruded as described in **Section: 2.10. Bioprinting Protocol with cells**. Their growth was monitored for up to 7 days, with media refreshed every 3 days. Cell morphology and proliferation were obtained via confocal imaging at 24 hours, 72 hours, and 7 days of culture. The protocol used for this experiment is shown in **Figure 5 b.** and is described above.

With the hydrogel 2.5 mg.mL^{-1},after 24 h, as shown in **Figure 14 a.**, cells began to elongate and spread, displaying a relatively similar morphology. After 72 h of culture, as shown in **Figure 14 b.,** cells exhibited further morphological changes and began forming intercellular connections, suggesting active communication and adaptation to the microenvironment.

Unfortunately, for day 7, we encountered a technical issue with the green dye, and it was too late to repeat the experiment another time.

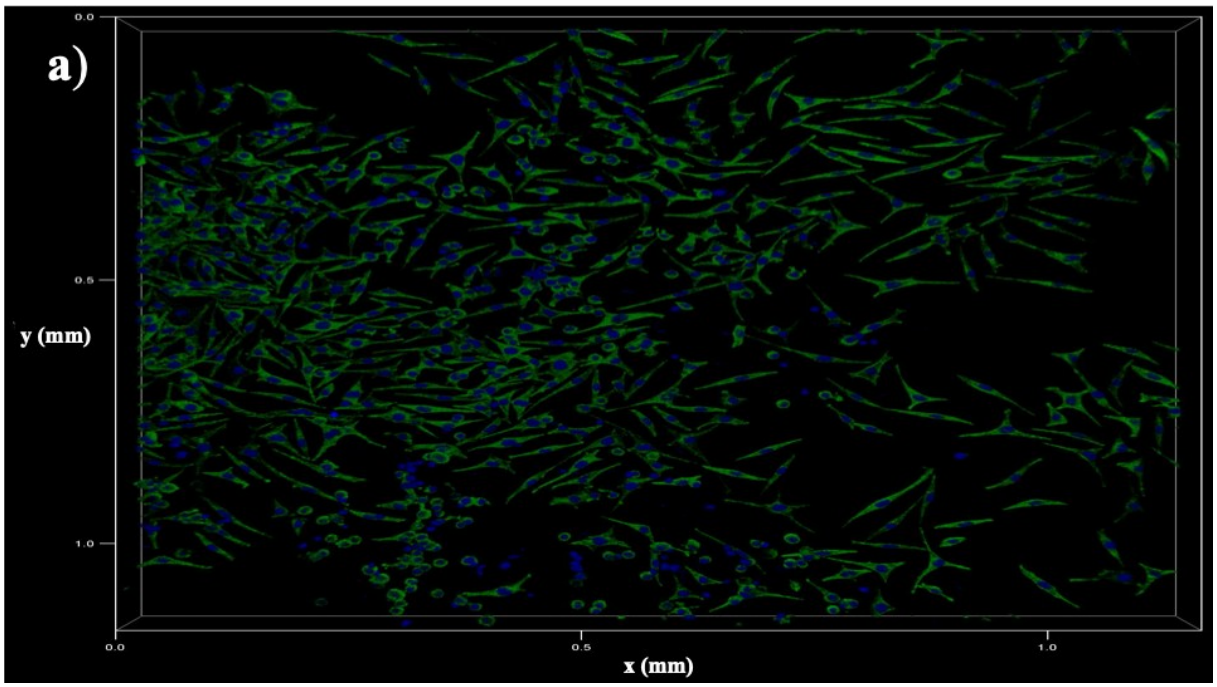

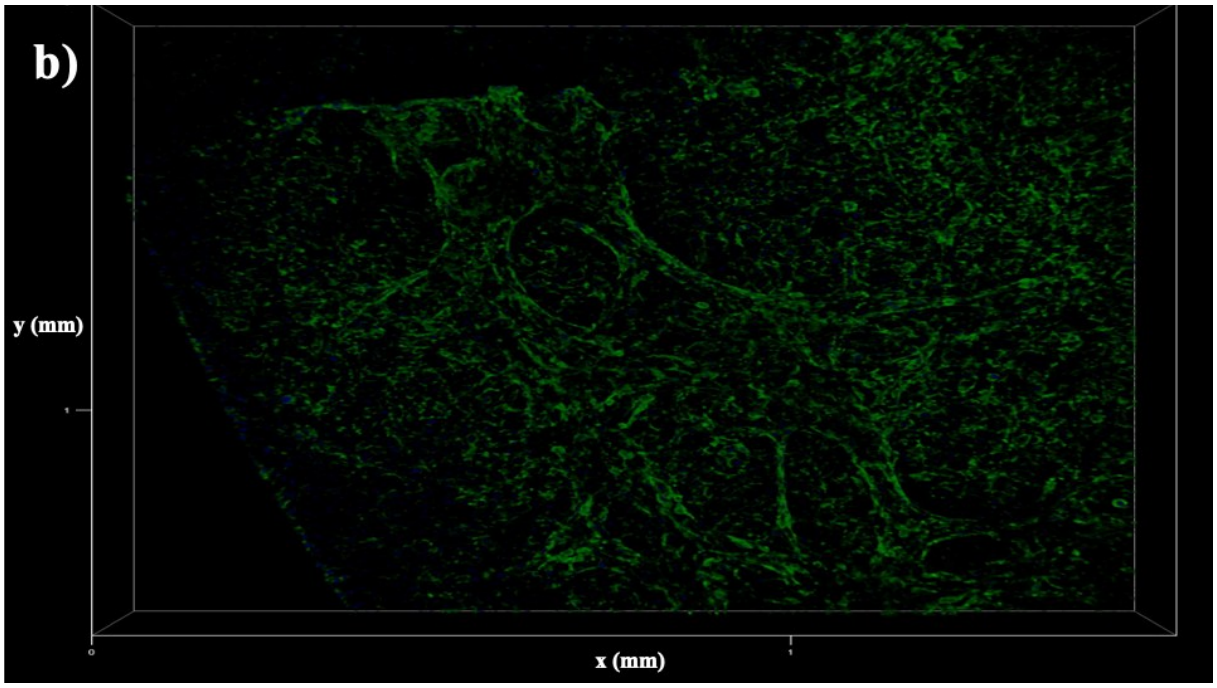

Figure 14 - 3D projection of confocal microscope imaging of L929 fibroblasts cultivated on top of 2.5 mg.mL^{-1} dECM hydrogel. a) after 24 h of culture, b) after 72 h of culture.

4. Conclusion and Future Work

The goal of this work was to develop a bioprinting protocol that ensures high cell viability and improved shape fidelity, envisioning their use in 3D bioprinting and tissue engineering applications. For this, we started by decellularizing extracellular matrix derived from porcine skin to formulate a hydrogel suitable for extrusion-based 3D bioprinting.

It was confirmed that the previously established decellularization protocol is reproducible, effectively removing cellular content while preserving essential ECM components such as collagen, elastin, GAGs, and DNA. Biochemical quantifications confirmed the efficiency and consistency of the protocol, with results comparable to previously published data.

All dECM hydrogels at a concentration of 2.5 $mg.mL^{-1}$ exhibited shear-thinning behavior and gelation properties compatible with extrusion-based printing. For printing experiments, we tested different needle gauges, and according to the filament width 23G was the best needle tip in terms of extrudability of the filament.

Finally, in vitro culture of fibroblasts on the hydrogel showed promising initial cell spreading and network formation after 24 and 72 hours. However, results for 7 day of culture were not obtained within the timeframe of this study. The development of the protocol itself was intensive and time-consuming, requiring considerable trial-and-error approaches, multiple observations, and setbacks with subsequent readjustments to finally achieve reproducible results in a reliable manner. In future work, we intend to incorporate a crosslinker, such as genipin, to further enhance the mechanical properties of the hydrogel; however, this could not be achieved due to time constraints [48].

Considering all these results, these findings demonstrate that this study represents a promising approach for bioprinting applications. Nevertheless, additional research is required to improve the mechanical stability.

5. References

(1) Kupiec-Weglinski, J. W. Grand Challenges in Organ Transplantation. *Front. Transplant.* **2022**, *1*. https://doi.org/10.3389/frtra.2022.897679.

(2) European Comisison. Blood, Tissues, Cells and Organs, 2023. https://health.ec.europa.eu/blood-tissues-cells-and-organs/organs_en.

(3) Carrier, A. N.; Verma, A.; Mohiuddin, M.; Pascual, M.; Muller, Y. D.; Longchamp, A.; Bhati, C.; Buhler, L. H.; Maluf, D. G.; Meier, R. P. H. Xenotransplantation: A New Era. *Front. Immunol.* **2022**, *13*, 900594. https://doi.org/10.3389/fimmu.2022.900594.

(4) Langer, R.; Vacanti, J. P. Tissue Engineering. *Science* **1993**, *260* (5110), 920–926. https://doi.org/10.1126/science.8493529.

(5) Yao, Q.; Zheng, Y.-W.; Lan, Q.-H.; Kou, L.; Xu, H.-L.; Zhao, Y.-Z. Recent Development and Biomedical Applications of Decellularized Extracellular Matrix Biomaterials. *Mater. Sci. Eng. C Mater. Biol. Appl.* **2019**, *104*, 109942. https://doi.org/10.1016/j.msec.2019.109942.

(6) Toprakhisar, B.; Nadernezhad, A.; Bakirci, E.; Khani, N.; Skvortsov, G. A.; Koc, B. Development of Bioink from Decellularized Tendon Extracellular Matrix for 3D Bioprinting. *Macromol. Biosci.* **2018**, *18* (10), 1800024. https://doi.org/10.1002/mabi.201800024.

(7) Comprehensive Cancer Information - NCI. Extracellular Matrix; 2025.

(8) Kleinman, H. K.; Philp, D.; Hoffman, M. P. Role of the Extracellular Matrix in Morphogenesis. *Curr. Opin. Biotechnol.* **2003**, *14* (5), 526–532. https://doi.org/10.1016/j.copbio.2003.08.002.

(9) Yao, Q.; Zheng, Y.-W.; Lan, Q.-H.; Kou, L.; Xu, H.-L.; Zhao, Y.-Z. Recent Development and Biomedical Applications of Decellularized Extracellular Matrix Biomaterials. *Mater. Sci. Eng. C Mater. Biol. Appl.* **2019**, *104*, 109942. https://doi.org/10.1016/j.msec.2019.109942.

(10) Frantz, C.; Stewart, K. M.; Weaver, V. M. The Extracellular Matrix at a Glance. *J. Cell Sci.* **2010**, *123* (24), 4195–4200. https://doi.org/10.1242/jcs.023820.

(11) Ottani, V.; Martini, D.; Franchi, M.; Ruggeri, A.; Raspanti, M. Hierarchical Structures in Fibrillar Collagens. *Micron Oxf. Engl. 1993* **2002**, *33* (7–8), 587–596. https://doi.org/10.1016/s0968-4328(02)00033-1.

(12) Pati, F.; Jang, J.; Ha, D.-H.; Won Kim, S.; Rhie, J.-W.; Shim, J.-H.; Kim, D.-H.; Cho, D.-W. Printing Three-Dimensional Tissue Analogues with Decellularized Extracellular Matrix Bioink. *Nat. Commun.* **2014**, *5*, 3935. https://doi.org/10.1038/ncomms4935.

(13) Van Der Rest, M.; Garrone, R. Collagen Family of Proteins. *FASEB J.* **1991**, *5* (13), 2814–2823. https://doi.org/10.1096/fasebj.5.13.1916105.

(14) Raines, E. W. The Extracellular Matrix Can Regulate Vascular Cell Migration, Proliferation, and Survival: Relationships to Vascular Disease. *Int. J. Exp. Pathol.* **2000**, *81* (3), 173–182. https://doi.org/10.1046/j.1365-2613.2000.00155.x.

(15) Ratcliffe, A. Tissue Engineering of Vascular Grafts. *Matrix Biol. J. Int. Soc. Matrix Biol.* **2000**, *19* (4), 353–357. https://doi.org/10.1016/s0945-053x(00)00080-9.

(16) Hwang, N. S.; Varghese, S.; Lee, H. J.; Theprungsirikul, P.; Canver, A.; Sharma, B.; Elisseeff, J. Response of Zonal Chondrocytes to Extracellular Matrix-Hydrogels. *FEBS Lett.* **2007**, *581* (22), 4172–4178. https://doi.org/10.1016/j.febslet.2007.07.049.

(17) Pavesio, A.; Abatangelo, G.; Borrione, A.; Brocchetta, D.; Hollander, A. P.; Kon, E.; Torasso, F.; Zanasi, S.; Marcacci, M. Hyaluronan-Based Scaffolds (Hyalograft C) in the Treatment of Knee Cartilage Defects: Preliminary Clinical Findings. *Novartis Found. Symp.* **2003**, *249*, 203–217; discussion 229-233, 234–238, 239–241.

(18) Varghese, S.; Hwang, N. S.; Canver, A. C.; Theprungsirikul, P.; Lin, D. W.; Elisseeff, J. Chondroitin Sulfate Based Niches for Chondrogenic Differentiation of Mesenchymal Stem Cells. *Matrix Biol. J. Int. Soc. Matrix Biol.* **2008**, *27* (1), 12–21. https://doi.org/10.1016/j.matbio.2007.07.002.

(19) Hynes, R. O. Structure of Fibronectins. In *Fibronectins*; Rich, A., Series Ed.; Springer Series in Molecular Biology; Springer New York: New York, NY, 1990; pp 113–175. https://doi.org/10.1007/978-1-4612-3264-3_6.

(20) Kubota, Y.; Kleinman, H. K.; Martin, G. R.; Lawley, T. J. Role of Laminin and Basement Membrane in the Morphological Differentiation of Human Endothelial Cells into Capillary-like Structures. *J. Cell Biol.* **1988**, *107* (4), 1589–1598. https://doi.org/10.1083/jcb.107.4.1589.

(21) White, E. S.; Baralle, F. E.; Muro, A. F. New Insights into Form and Function of Fibronectin Splice Variants. *J. Pathol.* **2008**, *216* (1), 1–14. https://doi.org/10.1002/path.2388.

(22) Poole, J. J. A.; Mostaço-Guidolin, L. B. Optical Microscopy and the Extracellular Matrix Structure: A Review. *Cells* **2021**, *10* (7), 1760. https://doi.org/10.3390/cells10071760.

(23) Crapo, P. M.; Gilbert, T. W.; Badylak, S. F. An Overview of Tissue and Whole Organ Decellularization Processes. *Biomaterials* **2011**, *32* (12), 3233–3243. https://doi.org/10.1016/j.biomaterials.2011.01.057.

(24) Abaci, A.; Guvendiren, M. Designing Decellularized Extracellular Matrix-Based Bioinks for 3D Bioprinting. *Adv. Healthc. Mater.* **2020**, *9* (24), e2000734. https://doi.org/10.1002/adhm.202000734.

(25) Choudhury, D.; Yee, M.; Sheng, Z. L. J.; Amirul, A.; Naing, M. W. Decellularization Systems and Devices: State-of-the-Art. *Acta Biomater.* **2020**, *115*, 51–59. https://doi.org/10.1016/j.actbio.2020.07.060.

(26) Gilbert, T.; Sellaro, T.; Badylak, S. Decellularization of Tissues and Organs. *Biomaterials* **2006**, S0142961206001682. https://doi.org/10.1016/j.biomaterials.2006.02.014.

(27) Jiang, S.; Zhuang, Y.; Cai, M.; Wang, X.; Lin, K. Decellularized Extracellular Matrix: A Promising Strategy for Skin Repair and Regeneration. *Eng. Regen.* **2023**, *4* (4), 357–374. https://doi.org/10.1016/j.engreg.2023.05.001.

(28) Zhang, W.; Du, A.; Liu, S.; Lv, M.; Chen, S. Research Progress in Decellularized Extracellular Matrix-Derived Hydrogels. *Regen. Ther.* **2021**, *18*, 88–96. https://doi.org/10.1016/j.reth.2021.04.002.

(29) Porzionato, A.; Stocco, E.; Barbon, S.; Grandi, F.; Macchi, V.; De Caro, R. Tissue-Engineered Grafts from Human Decellularized Extracellular Matrices: A Systematic Review and Future Perspectives. *Int. J. Mol. Sci.* **2018**, *19* (12), 4117. https://doi.org/10.3390/ijms19124117.

(30) Garreta, E.; Oria, R.; Tarantino, C.; Pla-Roca, M.; Prado, P.; Fernández-Avilés, F.; Campistol, J. M.; Samitier, J.; Montserrat, N. Tissue Engineering by Decellularization and 3D Bioprinting. *Mater. Today* **2017**, *20* (4), 166–178. https://doi.org/10.1016/j.mattod.2016.12.005.

(31) Liu, B.; Zhang, S.; Wang, W.; Yun, Z.; Lv, L.; Chai, M.; Wu, Z.; Zhu, Y.; Ma, J.; Leng, L. Matrisome Provides a Supportive Microenvironment for Skin Functions of Diverse Species. *ACS Biomater. Sci. Eng.* **2020**, *6* (10), 5720–5733. https://doi.org/10.1021/acsbiomaterials.0c00479.

(32) Li, C.; An, N.; Song, Q.; Hu, Y.; Yin, W.; Wang, Q.; Le, Y.; Pan, W.; Yan, X.; Wang, Y.; Liu, J. Enhancing Organoid Culture: Harnessing the Potential of Decellularized Extracellular Matrix Hydrogels for Mimicking Microenvironments. *J. Biomed. Sci.* **2024**, *31* (1), 96. https://doi.org/10.1186/s12929-024-01086-7.

(33) Murphy, S. V.; Atala, A. 3D Bioprinting of Tissues and Organs. *Nat. Biotechnol.* **2014**, *32* (8), 773–785. https://doi.org/10.1038/nbt.2958.

(34) Ozbolat, I. T.; Hospodiuk, M. Current Advances and Future Perspectives in Extrusion-Based Bioprinting. *Biomaterials* **2016**, *76*, 321–343. https://doi.org/10.1016/j.biomaterials.2015.10.076.

(35) Abaci, A.; Guvendiren, M. Designing Decellularized Extracellular Matrix-Based Bioinks for 3D Bioprinting. *Adv. Healthc. Mater.* **2020**, *9* (24), e2000734. https://doi.org/10.1002/adhm.202000734.

(36) Stepanovska, J.; Supova, M.; Hanzalek, K.; Broz, A.; Matejka, R. Collagen Bioinks for Bioprinting: A Systematic Review of Hydrogel Properties, Bioprinting Parameters, Protocols, and Bioprinted Structure Characteristics. *Biomedicines* **2021**, *9* (9), 1137. https://doi.org/10.3390/biomedicines9091137.

(37) Engberg, A.; Stelzl, C.; Eriksson, O.; O'Callaghan, P.; Kreuger, J. An Open Source Extrusion Bioprinter Based on the E3D Motion System and Tool Changer to Enable FRESH and Multimaterial Bioprinting. *Sci. Rep.* **2021**, *11* (1), 21547. https://doi.org/10.1038/s41598-021-00931-1.

(38) Kort-Mascort, J.; Flores-Torres, S.; Peza-Chavez, O.; Jang, J. H.; Pardo, L. A.; Tran, S. D.; Kinsella, J. Decellularized ECM Hydrogels: Prior Use Considerations, Applications, and Opportunities in Tissue Engineering and Biofabrication. *Biomater. Sci.* **2023**, *11* (2), 400–431. https://doi.org/10.1039/D2BM01273A.

(39) Saldin, L. T.; Cramer, M. C.; Velankar, S. S.; White, L. J.; Badylak, S. F. Extracellular Matrix Hydrogels from Decellularized Tissues: Structure and Function. *Acta Biomater.* **2017**, *49*, 1–15. https://doi.org/10.1016/j.actbio.2016.11.068.

(40) Palierse, E.; Mihailescu, A. M.; Bergquist, I.; Persson, C.; Aramesh, M. Tuning the Mechanical Properties and Printability of Viscoelastic Skin-Derived Hydrogels for 3D Cell Culture. Bioengineering March 14, 2025. https://doi.org/10.1101/2025.03.12.642751.

(41) August Claesson & Karl Vilhelm Ståhl. *Decellularized Extracellular Matrix as Bioink for 3D Printing*; 2024. https://www.diva-portal.org/smash/get/diva2:1892589/FULLTEXT01.pdf.

(42) Voytik-Harbin, S. L.; Rajwa, B.; Robinson, J. P. Chapter 27 Three-Dimensional Imaging of Extracellular Matrix and Extracellular Matrix-Cell Interactions. In *Methods in Cell Biology*; Elsevier, 2001; Vol. 63, pp 583–597. https://doi.org/10.1016/S0091-679X(01)63031-0.

(43) Girardeau-Hubert, S.; Lynch, B.; Zuttion, F.; Label, R.; Rayee, C.; Brizion, S.; Ricois, S.; Martinez, A.; Park, E.; Kim, C.; Marinho, P. A.; Shim, J.-H.; Jin, S.; Rielland, M.; Soeur, J. Impact of Microstructure on Cell Behavior and Tissue Mechanics in Collagen and Dermal Decellularized Extra-Cellular Matrices. *Acta Biomater.* **2022**, *143*, 100–114. https://doi.org/10.1016/j.actbio.2022.02.035.

(44) Wolf, M. T.; Daly, K. A.; Brennan-Pierce, E. P.; Johnson, S. A.; Carruthers, C. A.; D'Amore, A.; Nagarkar, S. P.; Velankar, S. S.; Badylak, S. F. A Hydrogel Derived from Decellularized Dermal Extracellular Matrix. *Biomaterials* **2012**, *33* (29), 7028–7038. https://doi.org/10.1016/j.biomaterials.2012.06.051.

(45) Xu, P.; Kankala, R. K.; Wang, S.; Chen, A. Decellularized Extracellular Matrix-Based Composite Scaffolds for Tissue Engineering and Regenerative Medicine. *Regen. Biomater.* **2024**, *11*, rbad107. https://doi.org/10.1093/rb/rbad107.

(46) Ouyang, L.; Yao, R.; Zhao, Y.; Sun, W. Effect of Bioink Properties on Printability and Cell Viability for 3D Bioplotting of Embryonic Stem Cells. *Biofabrication* **2016**, *8* (3), 035020. https://doi.org/10.1088/1758-5090/8/3/035020.

(47) Poon, C. Measuring the Density and Viscosity of Culture Media for Optimized Computational Fluid Dynamics Analysis of in Vitro Devices. *J. Mech. Behav. Biomed. Mater.* **2022**, *126*, 105024. https://doi.org/10.1016/j.jmbbm.2021.105024.

(48) Výborný, K.; Vallová, J.; Kočí, Z.; Kekulová, K.; Jiráková, K.; Jendelová, P.; Hodan, J.; Kubinová, Š. Genipin and EDC Crosslinking of Extracellular Matrix Hydrogel Derived from Human Umbilical Cord for Neural Tissue Repair. *Sci. Rep.* **2019**, *9* (1). https://doi.org/10.1038/s41598-019-47059-x.